Defense Technical Information Center Compilation Part Notice

ADP012246

TITLE: Analysis of the Atomic-Scale Defect Chemistry at Interfaces in Fluorite Structured Oxides by Electron Energy Loss Spectroscopy

DISTRIBUTION: Approved for public release, distribution unlimited

This paper is part of the following report:

TITLE: Nanophase and Nanocomposite Materials IV held in Boston, Massachusetts on November 26-29, 2001

To order the complete compilation report, use: ADA401575

The following component part numbers comprise the compilation report:
ADP012174 thru ADP012259

Mat. Res. Soc. Symp. Proc. Vol. 703 © 2002 Materials Research Society V11.10

ANALYSIS OF THE ATOMIC-SCALE DEFECT CHEMISTRY AT INTERFACES IN FLUORITE STRUCTURED OXIDES BY ELECTRON ENERGY LOSS SPECTROSCOPY

Y. Ito, Y Lei[1], N.D. Browning[1] and T.J. Mazanec[2]

Department of Physics, Northern Illinois University, DeKalb, IL 60115
[1]Department of Physics (M/C 273), University of Illinois at Chicago, Chicago, IL 60607
[2]BP Amoco Chemicals, Naperville, IL 60566-7011

ABSTRACT

Gd^{3+} doped Ce oxides are a major candidate for use as the electrolyte in solid oxide fuel cells operating at ~500 °C. Here, the effect of the atomic structure on the local electronic properties, i.e. oxygen coordination and cation valence, at grain boundaries in the fluorite structured $Gd_{0.2}Ce_{0.8}O_{2-x}$ ceramic electrolyte is investigated by a combination of atomic resolution Z-contrast imaging and electron energy loss spectroscopy (EELS) in the scanning transmission electron microscope (STEM). In particular, EELS analyses from grain boundaries reveals a complex interaction between segregation of the dopant (Gd^{3+}), oxygen vacancies and the valence state of Ce. These results are similar to observations from fluorite-structured Yttria-Stabilized Zirconium (YSZ) bicrystal grain boundaries.

INTRODUCTION

Gd^{3+} doped Ce oxides are highly attractive candidates as electrolytes for solid oxide fuel cells operating at ~500 °C [1,2]. Like YSZ, the high oxygen conductivity has a structural origin, i.e. the fluorite structure has the highest capacity for oxygen vacancies while the cation sublattice holds the cubic structure of the bulk without collapsing [3]. For their successful commercial implementation, a full understanding of the defect chemistry in the bulk and at grain boundaries is essential. In particular, the contribution of the grain boundaries to the total ionic conductivity through such effects as the segregation of dopants, vacancies and impurities is of crucial importance [4].

The route to characterizing oxide materials on this level is afforded by the combination of Z-contrast imaging [4] and EELS [5] in the STEM. These correlated techniques [6] allow direct images of crystal and defect structures to be obtained, the composition to be quantified and the effect of the structures on the local electronic properties (i.e., oxygen coordination and cation valence) to be assessed [7]. Here the effect of the atomic structure on the local electronic properties, i.e. oxygen coordination and cation valence at grain boundaries of the fluorite structured $Gd_{0.2}Ce_{0.8}O_{2-x}$ ceramic membrane material is investigated by a combination of Z-contrast imaging [5] and EELS [6] in the JEOL 2010F STEM [7]. These results are compared with atomic resolution Z-contrast imaging and EELS analyses of a model symmetric [001] tilt grain boundary YSZ [8]. The use of the model system for comparison is required to obtain a detailed understanding of the atomic scale phenomena in ceramics, as the polycrystalline nature of $Gd_{0.2}Ce_{0.8}O_{2-x}$ ceramic membrane material makes it almost impossible to locate the ideal zone-axis orientation required to image the boundary plane.

SPECIMEN

The composite membrane material consisting of polycrystalline $Gd_{0.2}Ce_{0.8}O_{2-x}$ and Pd metal grains was provided by BP Amoco Chemicals, which was sintered from high purity pre-mixed powders at high temperature with the Gd/Ce ratio of 0.2. (Pd permits the electrons to be transported). The oxygen permeation experiments were performed at 950°C where one face was in contact with air and the other was in contact with H_2/CO_2 with pO_2 = 1 x 10-15 atm (H_2/CO_2 = 85/15). For the present study, grain boundaries directly connected to Pd metal grains were excluded in order to characterize pure ceramic-ceramic grain boundaries (EELS and energy dispersive x-ray spectroscopy analysis confirmed the boundaries analyzed here were free from Pd). The YSZ symmetric 24° [001] tilt bicrystal stabilized in the cubic form with ~10 mol % Y_2O_3 doping was purchased from Shinkosha Co., Ltd. Japan. For both materials, TEM samples were prepared by standard procedures, mechanically polished and then thinned by argon ion milling to electron transparency.

EXPERIMENTAL TECHNIQUES

The experiments were performed on a 200kV Schottky field emission JEOL 2010F STEM/TEM at the University of Illinois at Chicago, equipped with an ultra high-resolution objective lens pole piece, a JEOL annular dark field detector (ADF) for Z-contrast imaging, and a Gatan imaging filter (GIF) for EELS [7]. In this study, a probe size of 0.2 nm with a convergence angle of 13 mrad was used. The inner radius of the ADF detector was 52 mrad. Due to the dominant contribution of Rutherford scattered electrons in this imaging condition, the image contrast is approximately proportional to Z^2 where Z is the atomic number. Consequently, more than 95% of the intensity in the Z-contrast images from these ceramic materials is due to electrons scattered by the cations and less than 5% from oxygen.

The low-angle scattered electrons, not intercepted by the ADF detector, were used for simultaneous EELS. EELS enables us to probe atomic scale fluctuations in composition and the effect of the local atomic structure on the electronic properties (i.e. oxygen coordination and cation valence) [9]. Energy shifts and the fine structure of the ionization edges reflect the atomic arrangement and bonding effects in the specimen. Combined with Z-contrast imaging in the STEM, it is possible to obtain spectra with atomic spatial resolution [6]. The Z-contrast image can therefore be used as a map to position the probe at the specified locations in the structure to obtain atomic scale information on the composition and bonding.

Each spectrum was acquired for 4 seconds for YSZ and 3 seconds for $Gd_{0.2}Ce_{0.8}O_{2-x}$, respectively. The probe position was checked after acquisition of each spectrum to make sure that the specimen drift was minimal (< 0.1 nm). A series of spectra were acquired at every position and summed up during post-acquisition data processing. This reduces the effects of drift and allows beam damage to be monitored (no appreciable beam damage was detected.). In all the spectra, plural scattering effects were removed by deconvolution with a low-loss spectrum [5].

RESULTS

YSZ grain boundary

A symmetric 24° [001] tilt YSZ grain boundary was investigated as a model fluorite structure grain boundary [8]. Figure 1(a) shows an atomic resolution Z-contrast image of the grain boundary. Bright spots in the image represent the cation sub-lattice (Zr and/or Y columns).

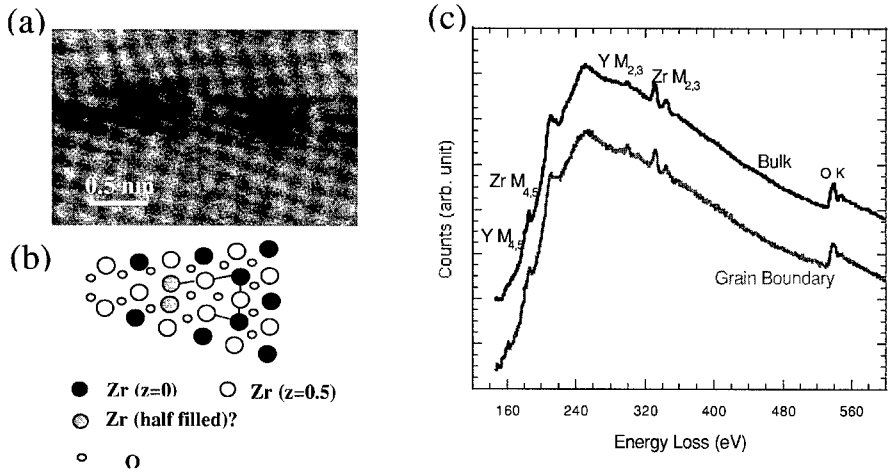

Figure 1: (a) Z-contrast image of a symmetric 24° [001] tilt grain boundary in YSZ. (b) a schematic of the grain boundary structure.[10] (c) EEL spectra from the bulk and grain boundary. Background before Y M_{45} is removed. [8]

Based on this Z-contrast image and the bulk crystal structure of YSZ, a possible schematic of the grain boundary atomic structure is shown in figure 1(b). This structure is consistent with previous analysis by Z-contrast imaging, and contains partially occupied columns [10]. Figure 1(c) shows the EEL spectra acquired from the bulk and grain boundary of YSZ. Main differences between the two spectra include (1) a 1.5 eV shift to higher energy of the Z_{23}-peak at the grain boundary, and (2) a change of the O K near-edge structure (not shown) (this change in bonding character is a sign of the distortion of cubic symmetry at the grain boundary [11]). In addition, at the grain boundary there is (3) an increase of Zr and Y M_3/M_2 ratio, (4) an increase of the Y/Zr ratio, and (5) a decrease of O/Zr and O/Y ratios. (1) and (3) indicate an increase in the number of electrons in the boundary plane. This is consistent with the excess segregation of O vacancies (5) although it is partially compensated by the segregation of Y (4). This may cause the increase of the number of electrons in the conduction band at the boundary.

$Gd_{0.2}Ce_{0.8}O_{2-x}$ grain boundary

Figure 2 shows typical O K- and Ce M_{45}-edges of bulk $Gd_{0.2}Ce_{0.8}O_{2-x}$. The principal features of the near-edge fine structure are clearly resolved. These are very similar to those of CeO_2 (Ce^{4+})[12]. The O K-edge of CeO_2 is due to transitions from the 1s ground state to the p-like component of hybrid Ce 4f and O 2p energy levels (pre-edge (A)) and to the unoccupied O 2p-like states hybridized with the crystal-field split Ce d-states, i.e. e_g (B) and t_{2g} (C). Notice that the O K-edge of bulk YSZ does not have the pre-edge equivalent to (A). The sharp Ce M_{45} peaks are due to transitions of 3d core electrons ($3d_{5/2}$ for M_5 and $3d_{3/2}$ for M_4 due to spin orbit coupling) to unoccupied states of f-like symmetry (the much weaker 3d → p edge is masked). The satellites (Y, Y') are thought to originate from transitions to 4f states in the conduction band, and these satellites have been used to estimate the degree of delocalization of the f-electrons (strong covalency hybridization between Ce 4f and O 2p).

Figure 3 shows the O K- and Ce M_{45}-edges across the grain boundary between Grain A and B. At the grain boundary there is, (1) a decrease of the pre-peak A and t_{2g} peak C, (2) an increase of Ce M_5/M_4 ratio and slight broadening of the peaks, (3) a chemical shift of Ce M_{45} to lower energy-loss (1.5 eV), and (4) a decrease of the satellite peaks Y and Y' of Ce M_{45}. (1) and (3) may indicate the reduction of O 2p-Ce d and O 2p-Ce 4f hybridization at the grain boundary, respectively. (2), (3) and (4) indicate increase of Ce^{3+} at the grain boundary. This is also consistent with the change of the O 2p hybridization.

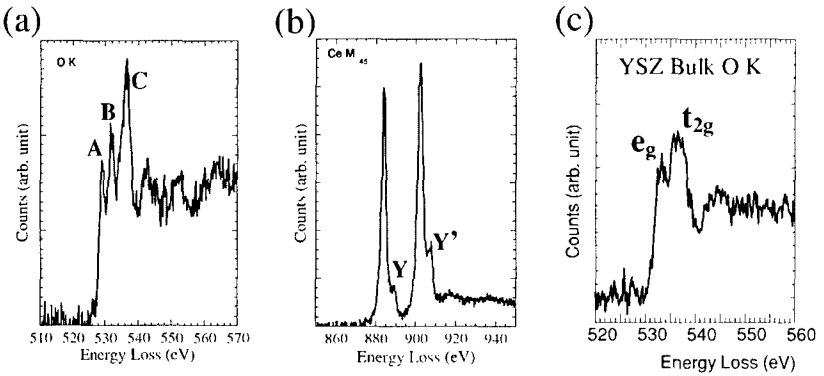

Figure 2: EEL spectra of bulk $Gd_{0.2}Ce_{0.8}O_{2-x}$ with high energy resolution. (a) O K-edge (b) Ce M_{45}-edges. (c) O K-edge of YSZ bulk for the comparison.

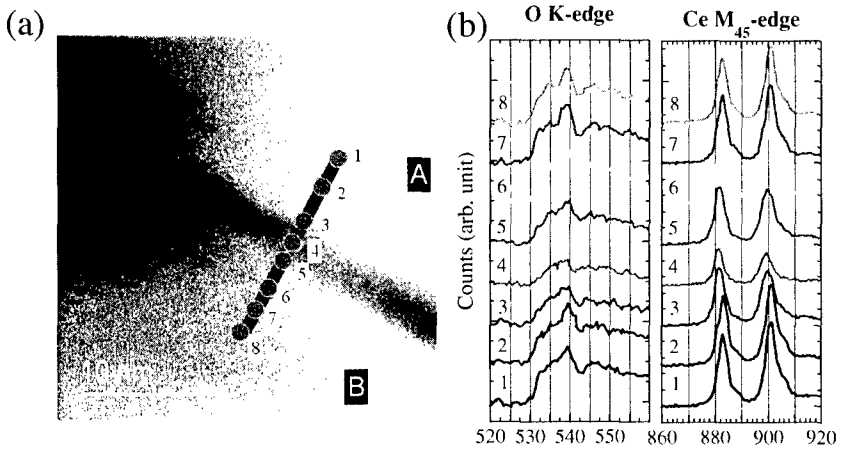

Figure 3: (a) Z-contrast image of a $Gd_{0.2}Ce_{0.8}O_{2-x}$ grain boundary (not aligned to a specific orientation but close to [110]). Points where EEL spectra were acquired are indicated. The numbers correspond to spectra in (b). (b) Oxygen K- and Ce M_{45}-EEL spectra across the grain boundary. Both O K- and Ce M_{45}-edges were acquired simultaneously.

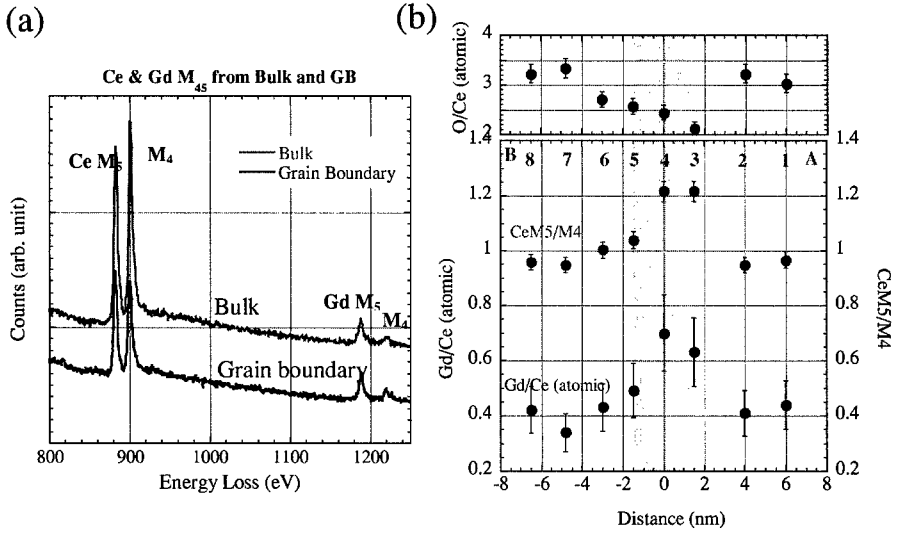

Figure 4: (a) Ce and Gd M_{45}-EEL spectra from the bulk and the grain boundary of a $Gd_{0.2}Ce_{0.8}O_{2-x}$. Both are on the same scale but shifted for the clarity. Same acquisition condition (b) The Ce M_5/M_4 ratio, Gd/Ce and O/Ce atomic ratios profiles across the grain boundary [8]. Numbers correspond to those in Figure 3.

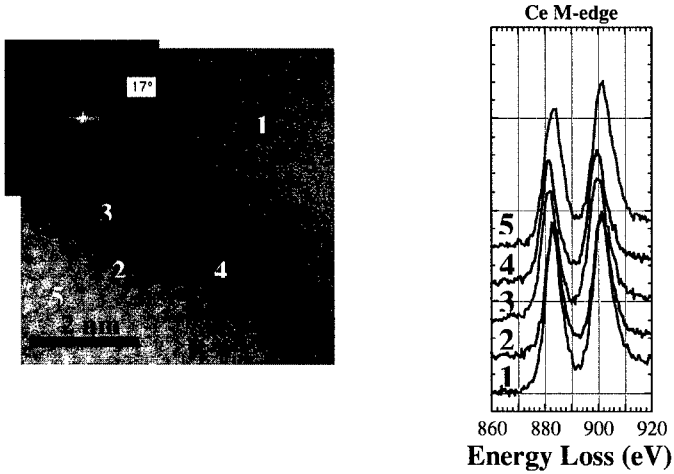

Figure 5: (a) Atomic resolution Z-contrast image of a $Gd_{0.2}Ce_{0.8}O_{2-x}$ grain boundary between grain A and B. (B is aligned to [110]). Points where EEL spectra were acquired are indicated. The numbers correspond to spectra in (b). The inset is a FFT of the image, indicating 17° tilt. (b) Ce M_{45}-EEL spectra around the grain boundary.

Figure 4 shows the segregation of the Gd and O vacancies at the grain boundaries and their close correlation with the change of the Ce M_5/M_4 ratio (valence state). The levels of Gd segregation and oxygen vacancies are similar to those in YSZ, and the effect on the Ce $M_{4,5}$-edge is analogous to that on the Zr $M_{2,3}$-edge. The composition at the grain boundary is calculated to be $Gd_{0.41\pm0.04}Ce_{0.59\pm0.04}O_{1.24\pm0.17}$. According to the reference of the M_5/M_4 values [13], the fraction of Ce^{3+} at the grain boundary is estimated to be 70% by assuming a linear interpolation. Therefore, for this grain boundary, the excess of electrons near the grain boundary in this sample was derived to be 0.7 ± 0.35 per formula unit.

The above results are also supported by the preliminary atomic resolution EELS analysis of the same boundary (Figure 5).

CONCLUSIONS

The interplay between oxygen vacancies, dopant distribution and valence state of Ce (Zr) at grain boundaries of the fluorite structured YSZ and $Gd_{0.2}Ce_{0.8}O_{2-x}$ ceramic electrolyte has been studied by a combination of atomic resolution Z-contrast imaging and EELS in a STEM. The majority of the grain boundaries exhibit segregation of Gd and oxygen vacancies. The Ce M_{45}-edge analyses indicate a decrease of the valence state. Observation of the O K-edge near-edge fine structure also indicates changes in local atomic environment between the bulk and the boundary, consistent with the change of the valence state of Ce. The results from the $Gd_{0.2}Ce_{0.8}O_{2-x}$ are consistent with those from YSZ grain boundary, implying that the present observation may be common features at the grain boundaries in many fluorite structure materials.

ACKNOWLEDGMENTS

The authors would like to acknowledge support from BP chemicals for this work. This work was sponsored by the Department of Energy under contract number DE-FG02-96ER40512. The JEOL 2010F used to obtain the experimental results was purchased with support from the National Science Foundation under grant number NSF-DMR-9601792, and is operated by the Research Resources Center at the University of Illinois at Chicago.

REFERENCES

[1] B. C. H. Steele, *J. Power Sources* **49,** 1 (1994).
[2] B. C. H. Steele, *Solid State Ionics* **129,** 95 (2000).
[3] Z. L. Wang and Z. C. Kang, *Functional and Smart Materials* (Plenum, 1998)
[4] S. J. Pennycook and D. E. Jesson, *Phys. Rev. Lett.* **64,** 938 (1990).
[5] R. F. Egerton, *Electron Energy Loss Spectroscopy in the Electron Microscope* (Plenum, 1996).
[6] N. D. Browning, M. F. Chisholm and S. J. Pennycook, *Nature* **366**, 143 (1993).
[7] E. M. James and N. D. Browning, *Ultramicroscopy* **78,** 125 (1999).
[8] Y. Lei, Y. Ito, N. D. Browning, T. J. Mazanec, *J. Am. Cer. Soc.* (2001) submitted.
[9] R. F. Klie and N. D. Browning, *Appl. Phys. Lett.* **77,** 3737 (2000).
[10] E. C. Dickey and X. Fan, *J. Am. Cer. Soc.* **84,** 1361 (2001).
[11] J. Yuan, T. Hirayama, Y. Ikuhara, and T. Sakuma, *Micron*, **30,** 141 (1999).
[12] L. A. J. Garvie and P. R. Buseck, *J. Phys. Chem. Solids.* **60,** 1943 (2000).
[13] J. A. Fortner and E. C. Buck, *Appl. Phys. Lett.*, **68,** 3817 (1996).